Electronic Supplementary Material (ESI) for Journal of Materials Chemistry A.

Electronic Supplementary Information for

Theoretical Investigation on Hydrogenation of Dinitrogen Triggered by Singly Dispersed Bimetallic Sites

Xue-Lu Ma [a*], Yue Yang [a], Le-Min Xu[a], Hai Xiao [b], Wen-Zhi Yao [c], Jun Li [b*]

a School of Chemical & Environmental Engineering, China University of Mining & Technology, Beijing 100083, China;

b Department of Chemistry and Key Laboratory of Organic Optoelectronics & Molecular Engineering of Ministry of Education, Tsinghua University, Beijing 100084, China;

c Department of Environmental and Municipal Engineering, North China University of Water Conservancy and Electric Power, Zhengzhou 450011, China.

* Corresponding author: maxl@cumtb.edu.cn; junli@tsinghua.edu.cn

Figure S1. Top view of the optimized geometries and the computed electron density difference maps of M_1Co_n/CoO_x SCCs.

Figure S2. Data of (a) the first ionization energies and (b) the electron affinity energies for 24 transition metals.

Figure S3. Projected density of states (PDOS) of the doped M d-orbitals and neighboring Co d-orbitals of M_1Co_n/CoO_x SCCs.

Figure S4. Projected density of states (PDOS) for bridging adsorption configurations of N_2 on M_1Co_n/CoO_x SCCs.

Figure S5. Top view of the optimized the bridging dinitrogen adsorption structures and the computed electron density difference maps of dinitrogen and M_1Co_n/CoO_x SCCs.

Figure S6. Side view of the optimized the end-on dinitrogen adsorption structures and the computed electron density difference maps of dinitrogen and M_1Co_n/CoO_x SCCs.

Figure S7. The thermodynamic advantage configurations for the co-adsorption of N_2 and H_2 on M_1Co_n/CoO_x SCCs.

Figure S8. The relationship between the energy of bridging nitrogen adsorption and the energy of bridging co-adsorption.

Figure S9. The complete reaction pathway for the N_2-to-NH_3 thermal conversion on the Pd_1Co_4/CoO_x SCC compared with the original Rh_1Co_3/CoO_x SCC.

Figure S10. The relationship between the reaction energy and Bader charge difference of the doped M in the process from **I** to **II**.

Table S1. The M−Co bond lengths in M_1Co_n/CoO_x SCCs.

Table S2. The adsorption energies and N-N bond lengths in bridging N_2, end-on N_2 and H_2 on M_1Co_n/CoO_x SCCs.

Table S3. The parameters of I_1, N, and μ for M_1Co_n/CoO_x SCCs.

Table S4. The relative energies of intermediates (E_I and E_{II}), transition state energies ($E_{TSI\text{-}II}$), the activation energies barriers (ΔE_a) and reaction energies (ΔE_r) for the first hydrogenation of N_2.

Table S5. The key bond lengths in the process from **I** to **II**.

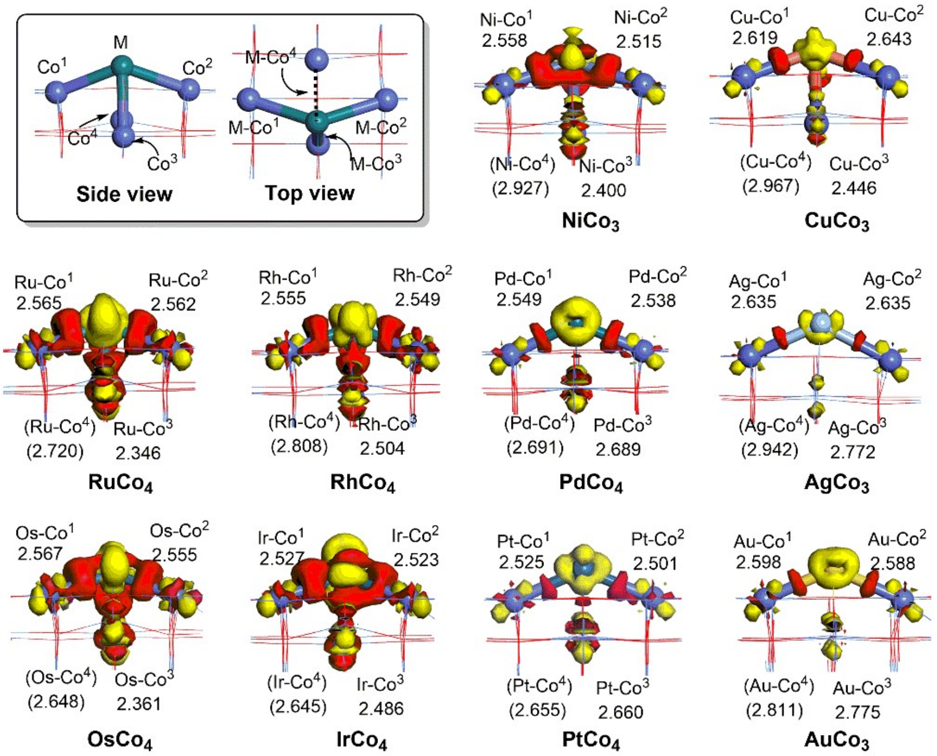

Figure S1. Top view of the optimized geometries and the computed electron density difference maps of M_1Co_n/CoO_x SCCs.

Note: The charge density difference was calculated by $\Delta\rho = \rho1 - \rho2 - \rho3$ (where $\rho1$, $\rho2$, and $\rho3$ represent the charge densities of the whole SCC system, CoO surface with O vacancy, and the doped metal, respectively). A decrease in electron density is shown in yellow and electron enrichment indicated in red (iso-value of 0.05 e/Å^3). The composition of the singly dispersed bimetallic cluster, M_1Co_n, can be referred to the distance (d_{MCo}) between the doped metal and neighboring Co atoms as listed in Table S1.

(a)The first ionization energy

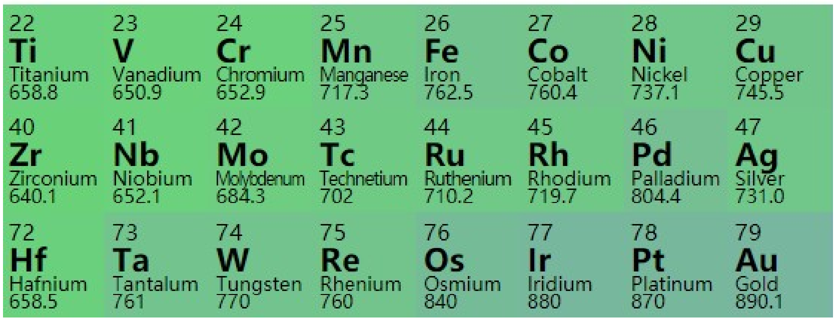

22 **Ti** Titanium 658.8	23 **V** Vanadium 650.9	24 **Cr** Chromium 652.9	25 **Mn** Manganese 717.3	26 **Fe** Iron 762.5	27 **Co** Cobalt 760.4	28 **Ni** Nickel 737.1	29 **Cu** Copper 745.5
40 **Zr** Zirconium 640.1	41 **Nb** Niobium 652.1	42 **Mo** Molybdenum 684.3	43 **Tc** Technetium 702	44 **Ru** Ruthenium 710.2	45 **Rh** Rhodium 719.7	46 **Pd** Palladium 804.4	47 **Ag** Silver 731.0
72 **Hf** Hafnium 658.5	73 **Ta** Tantalum 761	74 **W** Tungsten 770	75 **Re** Rhenium 760	76 **Os** Osmium 840	77 **Ir** Iridium 880	78 **Pt** Platinum 870	79 **Au** Gold 890.1

(b) The electron affinity energy

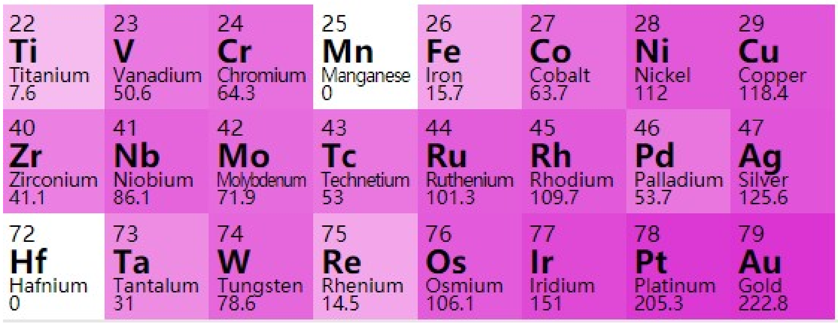

22 **Ti** Titanium 7.6	23 **V** Vanadium 50.6	24 **Cr** Chromium 64.3	25 **Mn** Manganese 0	26 **Fe** Iron 15.7	27 **Co** Cobalt 63.7	28 **Ni** Nickel 112	29 **Cu** Copper 118.4
40 **Zr** Zirconium 41.1	41 **Nb** Niobium 86.1	42 **Mo** Molybdenum 71.9	43 **Tc** Technetium 53	44 **Ru** Ruthenium 101.3	45 **Rh** Rhodium 109.7	46 **Pd** Palladium 53.7	47 **Ag** Silver 125.6
72 **Hf** Hafnium 0	73 **Ta** Tantalum 31	74 **W** Tungsten 78.6	75 **Re** Rhenium 14.5	76 **Os** Osmium 106.1	77 **Ir** Iridium 151	78 **Pt** Platinum 205.3	79 **Au** Gold 222.8

Figure S2. Data of (a) the first ionization energies and (b) the electron affinity energies for 24 transition metals. (From https://ptable.com/)

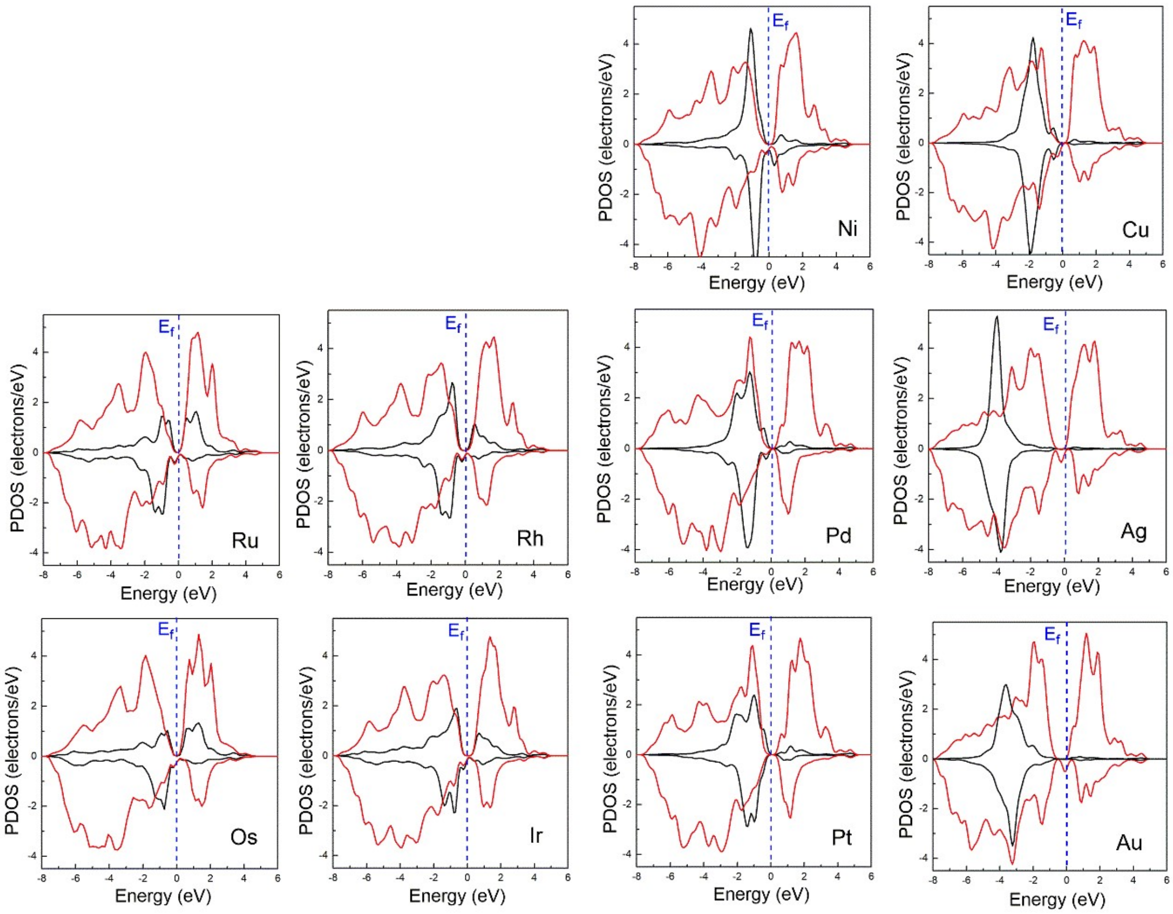

Figure S3. Projected density of states (PDOS) of the doped M d-orbitals and neighboring Co d-orbitals of M_1Co_n/CoO_x SCCs (M=Ni, Cu, Ru, Rh, Pd, Ag, Os, Ir, Pt, Au). The black and red lines are for the doped M atom and neighboring Co atoms, respectively. The positive and negative DOS denote the spin-up and spin-down states, respectively. The vertical dashed line indicates the Fermi level.

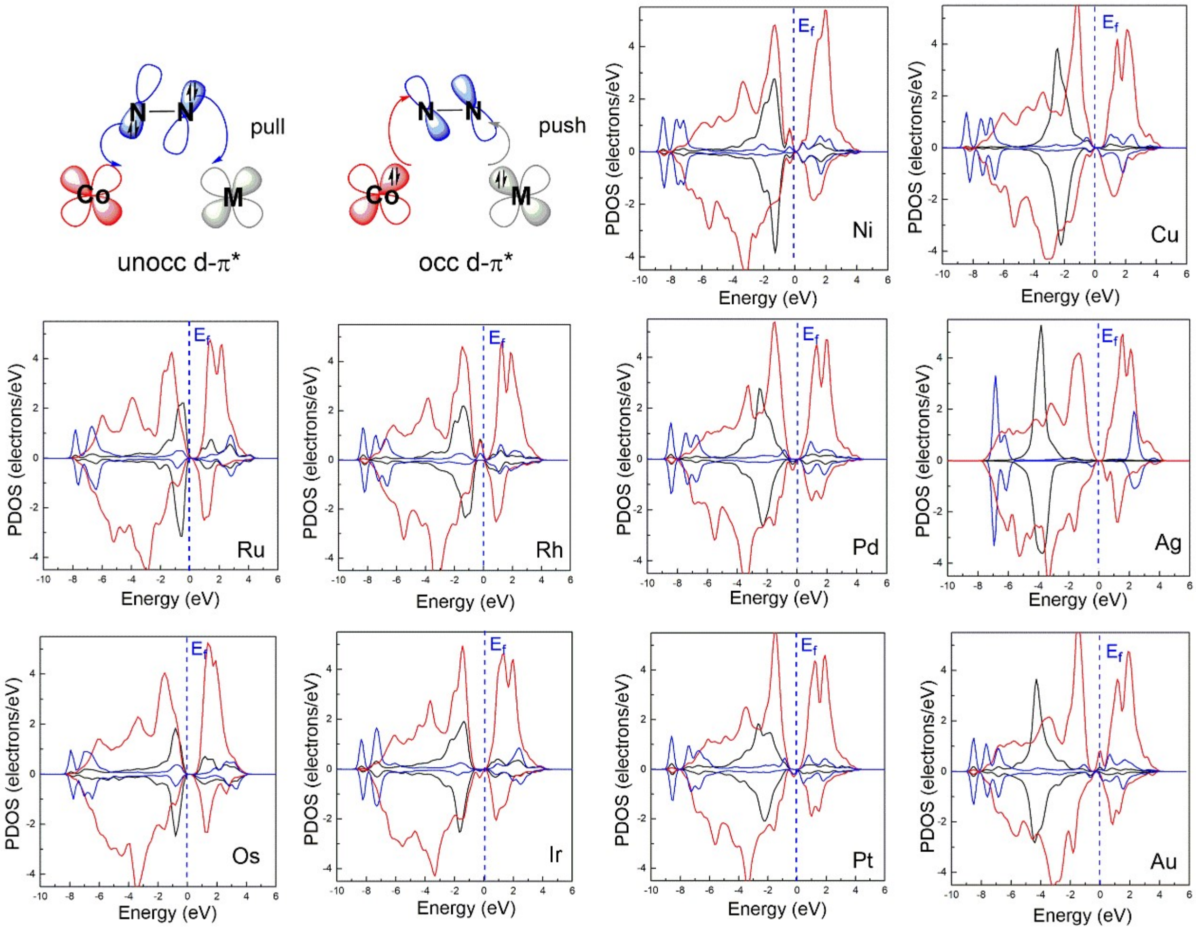

Figure S4. Projected density of states (PDOS) for bridging adsorption configurations of N_2 on M_1Co_n/CoO_x SCCs (M=Ni, Cu, Ru, Rh, Pd, Ag, Os, Ir, Pt, Au). The blue, black and red lines are for the dinitrogen unit, the doped M atom and neighboring Co atoms, respectively. The positive and negative DOS denote the spin-up and spin-down states, respectively. The vertical dashed line indicates the Fermi level.

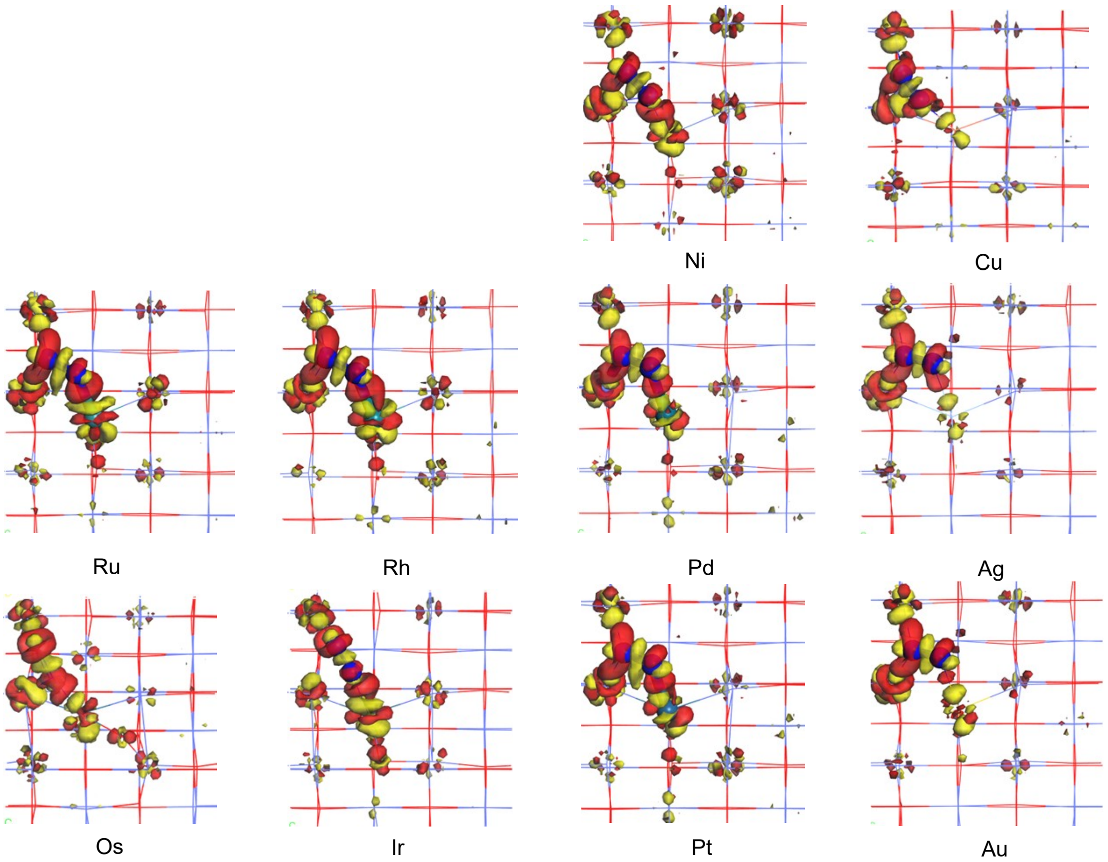

Ni Cu

Ru Rh Pd Ag

Os Ir Pt Au

Figure S5. Top view of the optimized the bridging dinitrogen adsorption structures and the computed electron density difference maps of dinitrogen and M_1Co_n/CoO_x SCCs (M=Ni, Cu, Ru, Rh, Pd, Ag, Os, Ir, Pt, Au).

Note: The charge density difference was calculated by $\Delta\rho = \rho1 - \rho2 - \rho3$ (where $\rho1$, $\rho2$, and $\rho3$ represent the charge densities of the whole system, M_1Co_n/CoO_x SCC, and the dinitrogen unit, respectively). A decrease in electron density is shown in yellow and electron enrichment indicated in red (iso-value of 0.05 e/Å^3).

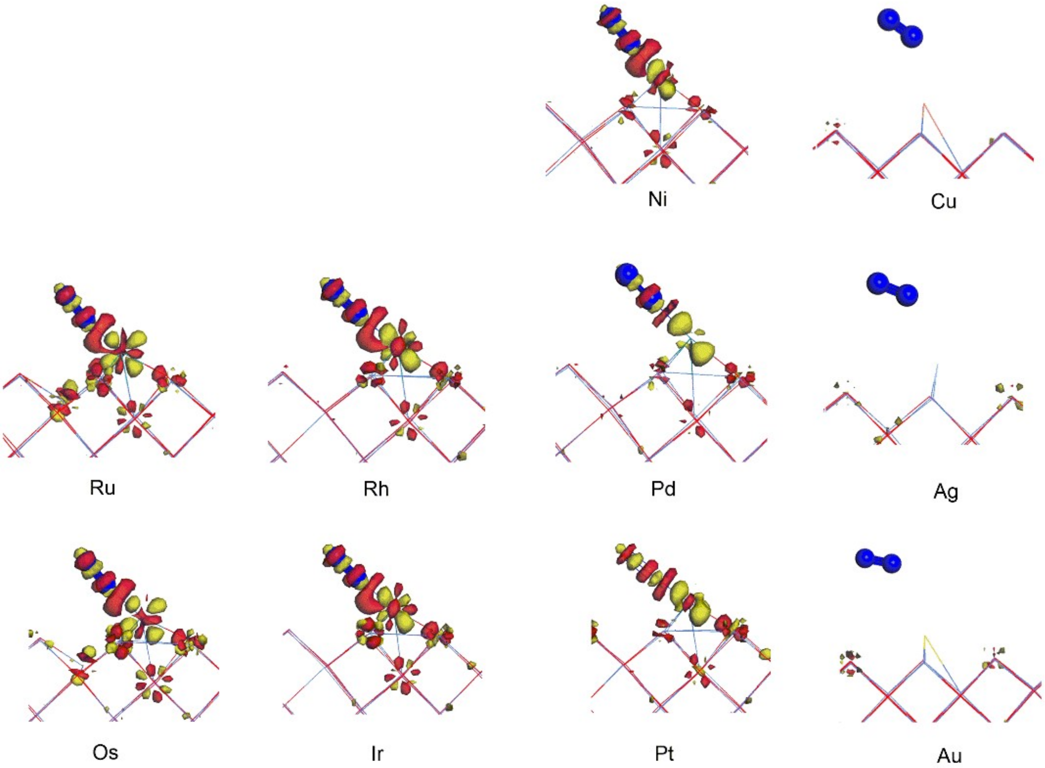

Figure S6. Side view of the optimized the end-on dinitrogen adsorption structures and the computed electron density difference maps of dinitrogen and M_1Co_n/CoO_x SCCs (M=Ni, Cu, Ru, Rh, Pd, Ag, Os, Ir, Pt, Au).

Note: The charge density difference was calculated by $\Delta\rho = \rho1 - \rho2 - \rho3$ (where $\rho1$, $\rho2$, and $\rho3$ represent the charge densities of the whole system, M_1Co_n/CoO_x SCC, and the dinitrogen unit, respectively). A decrease in electron density is shown in yellow and electron enrichment indicated in red (iso-value of 0.05 e/Å^3).

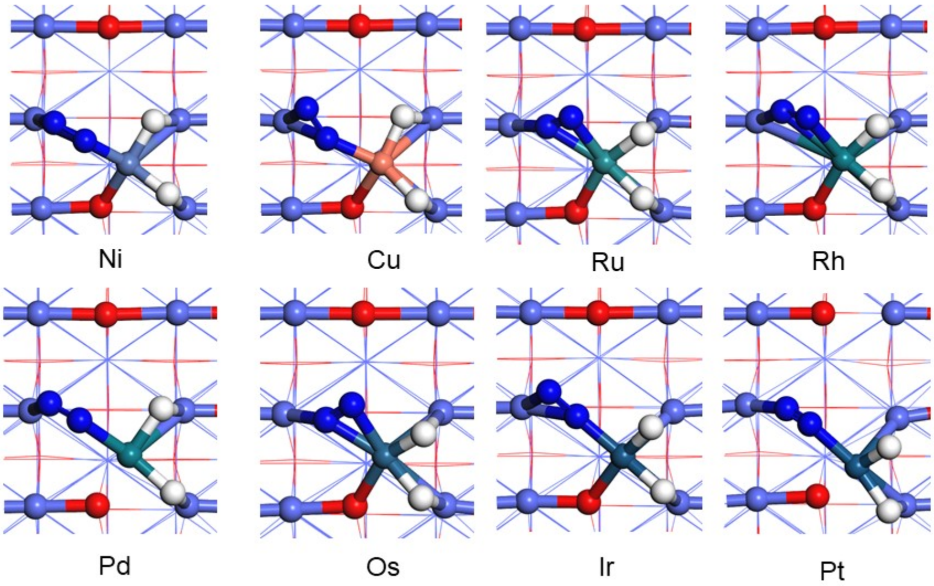

Figure S7. The thermodynamic advantage configurations for the co-adsorption of N_2 and H_2 on M_1Co_n/CoO_x SCCs (M=Ni, Cu, Ru, Rh, Pd, Os, Ir, Pt).

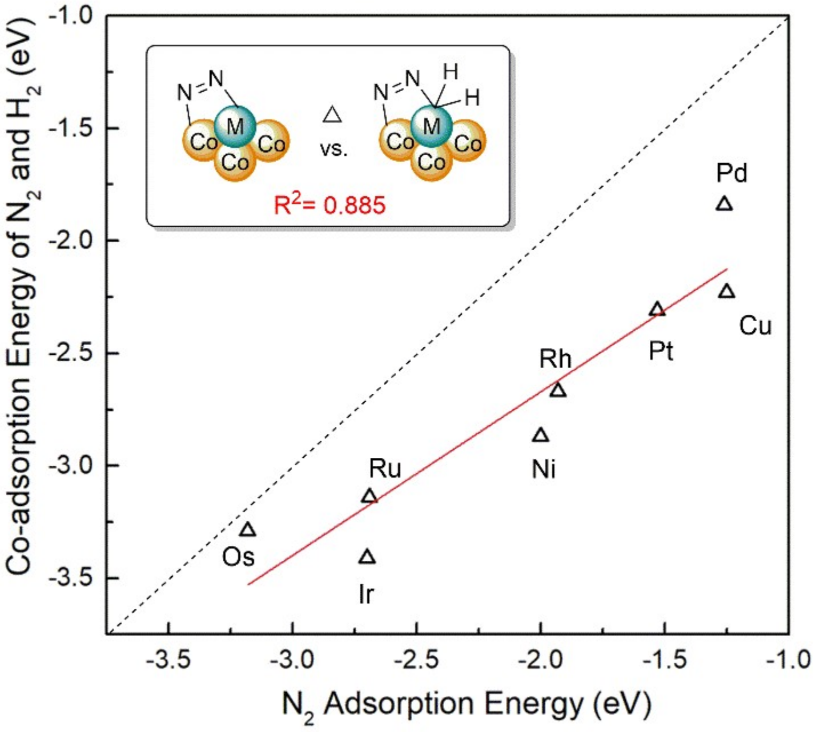

Figure S8. The relationship between the energy of bridging nitrogen adsorption and the energy of bridging co-adsorption.

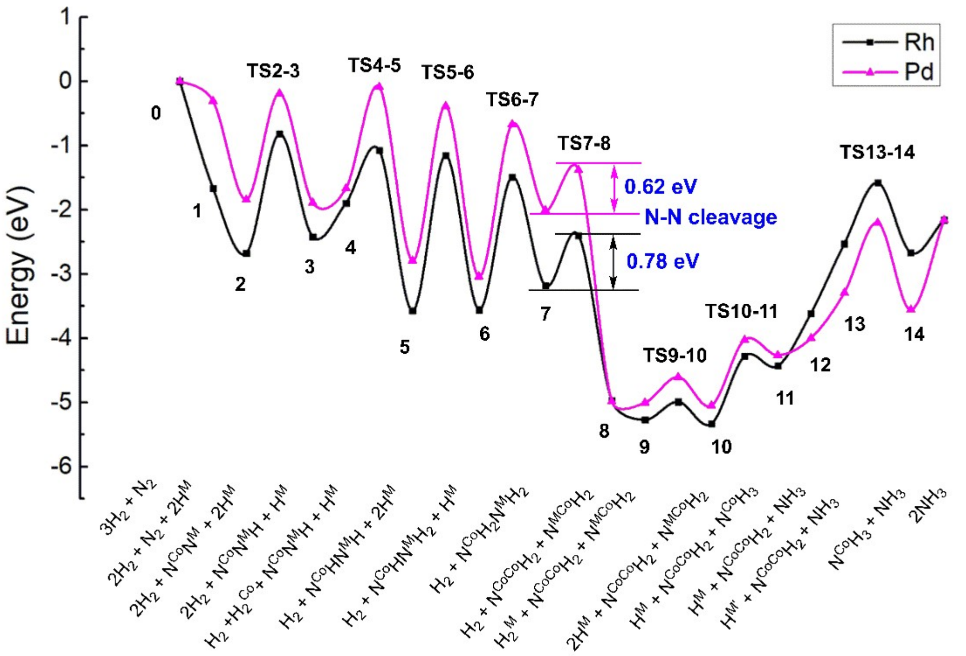

Figure S9. The complete reaction pathway for the N_2-to-NH_3 thermal conversion on the Pd_1Co_4/CoO_x SCC compared with the original Rh_1Co_3/CoO_x SCC.

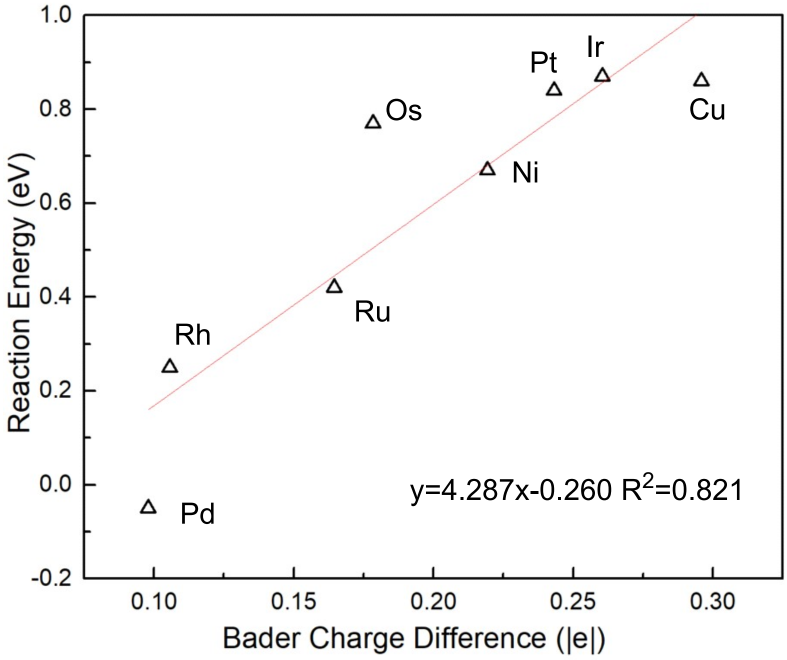

Figure S10. The relationship between the reaction energy and Bader charge difference of the doped M in the process from **I** to **II**.

Table S1. The M−Co bond lengths in M_1Co_n/CoO_x SCCs.

M_1Co_n/CoO_x SCC	d_{MCo_1}/Å	d_{MCo_2}/Å	d_{MCo_3}/Å	d_{MCo_4}/Å	R_{MCo}/Å	$\frac{d_{MCo_1}}{R_{AM}}$	$\frac{d_{MCo_2}}{R_{AM}}$	$\frac{d_{MCo_3}}{R_{AM}}$	$\frac{d_{MCo_4}}{R_{AM}}$
Ni_1Co_3/CoO_x	2.558	2.515	2.400	2.927	2.21	1.16	1.14	1.09	1.32
Cu_1Co_3/CoO_x	2.619	2.643	2.446	2.967	2.23	1.17	1.19	1.10	1.33
Ru_1Co_4/CoO_x	2.565	2.562	2.346	2.720	2.36	1.09	1.09	0.99	1.15
Rh_1Co_4/CoO_x	2.555	2.549	2.504	2.808	2.36	1.08	1.08	1.06	1.19
Pd_1Co_4/CoO_x	2.549	2.538	2.689	2.691	2.31	1.10	1.10	1.16	1.16
Ag_1Co_3/CoO_x	2.635	2.635	2.772	2.948	2.39	1.10	1.10	1.16	1.23
Os_1Co_4/CoO_x	2.567	2.555	2.361	2.648	2.40	1.07	1.06	0.98	1.10
Ir_1Co_4/CoO_x	2.527	2.523	2.486	2.645	2.33	1.08	1.08	1.07	1.14
Pt_1Co_4/CoO_x	2.525	2.501	2.660	2.655	2.34	1.08	1.07	1.14	1.13
Au_1Co_3/CoO_x	2.598	2.588	2.775	2.811	2.35	1.11	1.10	1.18	1.20

Note: The composition of the singly dispersed bimetallic cluster, M_1Co_n, can be referred to the distance (d_{MCo}) between the doped metal M and neighboring Co atoms. Here, if d_{MCo} is less than $1.2R_{MCo}$, where $R_{MCo} = r_M + r_{Co}$ is the sum of the Pyykkö radii of M and Co, this M is then considered to be bonded to the Co of CoO surface and included in the composition of cluster active site. Highlight that the representation of composition is related to the distance criterion to some extent.

Table S2. The adsorption energies and N-N bond lengths in bridging N_2, end-on N_2 and H_2 on M_1Co_n/CoO_x SCCs.

M_1Co_n/CoO_x SCC	Bridging N_2		End-on N_2		H_2
	$d_{N-N}/\text{Å}$	Ead/eV	$d_{N-N}/\text{Å}$	Ead/eV	Ead/eV
Ni_1Co_3/CoO_x	1.191	-2.00	1.140	-1.42	-1.63
Cu_1Co_3/CoO_x	1.192	-1.25	1.131	-0.41	-0.05
Ru_1Co_4/CoO_x	1.199	-2.69	1.147	-1.69	-1.57
Rh_1Co_4/CoO_x	1.200	-1.93	1.141	-1.66	-1.67
Pd_1Co_4/CoO_x	1.187	-1.26	1.132	-0.42	-0.31
Ag_1Co_3/CoO_x	1.183	-0.46	1.120	-0.17	NA
Os_1Co_4/CoO_x	1.201	-3.18	1.151	-1.71	-1.81
Ir_1Co_4/CoO_x	1.171	-2.70	1.146	-1.91	-1.95
Pt_1Co_4/CoO_x	1.205	-1.53	1.140	-0.65	-0.24
Au_1Co_3/CoO_x	1.183	-0.04	1.118	0.29	NA

Note: The adsorption energy is defined as: $E_{ad} = E_{SCC\text{-}N_2} - E_{SCC} - E_{N2}$, where E_{SCC} and $E_{SCC\text{-}N_2}$ represent the total energies of the bare M_1Co_n/CoO_x SCC and that with the adsorbed N_2 (SCC-N_2), respectively, and E_{N2} represents the total energy of a free N_2 molecule. This definition means that negative adsorption energy represents an exothermic process. The similar definition will be used for the H_2 adsorption and co-adsorption.

Table S3. The parameters of I_1, N, and μ for M_1Co_n/CoO_x SCCs.

M_1Co_n/CoO_x SCC	$I_1(kJ/mol)$	N	$\mu(kJ/mol)$
Ni_1Co_3/CoO_x	737.1	8	104.25
Cu_1Co_3/CoO_x	745.5	10	98.87
Ru_1Co_4/CoO_x	710.2	7	107.15
Rh_1Co_4/CoO_x	719.7	8	104.61
Pd_1Co_4/CoO_x	804.4	10	102.29
Ag_1Co_3/CoO_x	731.0	10	98.39
Os_1Co_4/CoO_x	840	6	114.28
Ir_1Co_4/CoO_x	880	7	111.85
Pt_1Co_4/CoO_x	870	9	106.12
Au_1Co_3/CoO_x	890.1	10	103.35

Table S4. The relative energies of intermediates (E_I and E_{II}), transition state energies (E_{TSI-II}), the activation energies barriers (ΔE_a) and reaction energies (ΔE_r) for the first hydrogenation of N_2. (Relative to the initial M_1Co_n/CoO_x SCCs and free molecules, unit: eV)

M_1Co_n/CoO_x SCC	E_I	E_{TSI-II}	E_{II}	ΔE_a	ΔE_r
Ni_1Co_3/CoO_x	-2.87	-0.81	-2.20	2.06	0.67
Cu_1Co_3/CoO_x	-2.23	0.03	-1.37	2.26	0.86
Ru_1Co_4/CoO_x	-3.14	-0.71	-2.72	2.43	0.42
Rh_1Co_4/CoO_x	-2.67	-0.82	-2.42	1.85	0.25
Pd_1Co_4/CoO_x	-1.84	-0.19	-1.89	1.65	-0.05
Os_1Co_4/CoO_x	-3.29	-0.83	-2.52	2.46	0.77
Ir_1Co_4/CoO_x	-3.41	-0.32	-2.54	3.09	0.87

Pt_1Co_4/CoO_x	-2.31	0.37	-1.47	2.68	0.84

Table S5. The key bond lengths in the process from **I** to **II**.

M_1Co_n/CoO_x SCC	d_{H-M}/Å□			d_{H-N}/Å□			d_{N-N}/Å			RMSD
	I	II	$\Delta_{H\text{-}N}$	I	II	$\Delta_{H\text{-}M}$	I	II	$\Delta_{N\text{-}N}$	
Ni_1Co_3/CoO_x	2.406	2.696	0.290	1.622	1.042	-0.580	1.172	1.268	0.096	0.378
Cu_1Co_3/CoO_x	2.583	2.649	0.066	1.645	1.049	-0.596	1.179	1.268	0.089	0.350
Ru_1Co_4/CoO_x	2.345	2.736	0.391	1.679	1.034	-0.645	1.190	1.268	0.078	0.438
Rh_1Co_4/CoO_x	2.351	2.743	0.392	1.623	1.036	-0.587	1.170	1.268	0.098	0.411
Pd_1Co_4/CoO_x	2.641	2.679	0.038	1.727	1.042	-0.685	1.167	1.268	0.101	0.400
Os_1Co_4/CoO_x	2.334	2.734	0.400	1.649	1.032	-0.617	1.221	1.268	0.047	0.425
Ir_1Co_4/CoO_x	2.488	2.740	0.252	1.699	1.035	-0.664	1.180	1.268	0.088	0.413
Pt_1Co_4/CoO_x	2.695	2.706	0.011	1.563	1.038	-0.525	1.164	1.268	0.104	0.309

$$\Delta = d_I - d_{II}$$

$$RMSD_{bond} = \sqrt{\frac{1}{3}({\Delta_{H-N}}^2 + {\Delta_{H-M}}^2 + {\Delta_{N-N}}^2)}$$